VNU Journal of Science: Mathematics - Physics

Journal homepage: https://js.vnu.edu.vn/MaP

Original Article

Pressure-driven Structural Transformation in the 9R Rhombohedral Phase of $BaMn_{0.85}Ti_{0.15}O_3$

Dang Ngoc Toan[1,*], Sergey E. Kichanov[2], Anton V. Rutkauskas[2], Hoang Trong Phuc[1], Dinh Thanh Khan[3], Trinh Ngoc Dat[3], Le Vu Truong Son[3], Phan The Long[4], Tran Tuan Anh[5]

[1]*Duy Tan University, 254 Nguyen Van Linh, Danang, Vietnam*

[2]*Frank Laboratory of Neutron Physics, Joint Institute for Nuclear Research, 141980 Dubna, Russia*

[3]*The University of Danang - University of Science and Education, 459 Ton Duc Thang, Danang, Vietnam*

[4]*VNU University of Engineering and Technology, 144 Xuan Thuy, Cau Giay, Hanoi, Vietnam*

[5]*Ho Chi Minh City University of Education and Technology, 1 Vo Van Ngan, Thu Duc, Ho Chi Minh City, Vietnam*

Received 01st July 2025
Revised 25th September 2025; Accepted 9th October 2025

Abstract: The high-pressure behavior of the 9R rhombohedral polymorph in $BaMn_{0.85}Ti_{0.15}O_3$ was investigated using synchrotron X-ray diffraction and Raman spectroscopy under compression up to 20.7 and 32.6 GPa, respectively. The 9R phase remains stable under pressure but exhibits anisotropic lattice compression, with the *c*-axis being less compressible due to intrinsic structural anisotropy. An isostructural transformation occurs around 9 GPa, as evidenced by anomalies in the pressure dependence of the lattice parameters, bulk modulus, and Raman vibrational modes. This transformation is attributed to pressure-driven rearrangements in the local bonding environment within the Mn/Ti–O octahedral framework, primarily involving Mn/Ti vibrations.

Keywords: Isostructural transformation, Raman spectroscopy, external pressure, X-ray diffraction.

1. Introduction

Multiferroic materials have emerged as a highly promising class of multifunctional systems owing to their potential applications in spintronics, advanced sensors, and next-generation memory devices, as

* Corresponding author.
E-mail address: dangngoctoan1@duytan.edu.vn

https//doi.org/10.25073/2588-1124/vnumap.5040

well as their importance in fundamental science [1-3]. The inherent interplay between the electronic, lattice, and spin degrees of freedom in these materials leads to a wide variety of unusual physical phenomena, including the magnetoelectric effect, giant thermal Hall effect, generation of electromagnons, spin-Peierls transitions, ultrafast magnetization dynamics, and the spin Seebeck effect, etc. [1-3]. In conventional multiferroics, the magnetoelectric (ME) coupling is generally very weak due to the fundamentally different origins of ferroelectricity and magnetism [1-3]. Conversely, improper multiferroics have demonstrated a pronounced ME coupling, where ferroelectricity emerges as a secondary outcome of magnetic ordering [4, 5]. In such systems, the magnetic structure breaks inversion symmetry, enabling the emergence of spontaneous electric polarization - often governed by mechanisms such as spin–orbit coupling or exchange striction [4, 5]. Nevertheless, a major challenge lies in the fact that both magnetic and ferroelectric transition temperatures in these systems are frequently far below room temperature, limiting their feasibility for real-world device integration.

In this context, numerous magnetoelectric phenomena have been discovered in polymorphs of $BaMnO_{3-\delta}$ and its derivatives. In particular, Korneta et al., [6] observed significant ME properties near room temperature in several antiferromagnetic phases, including 15R-$BaMnO_{2.99}$, 8H-$BaMn_{0.97}Li_{0.03}O_3$, and 12H-$BaMn_{0.97}K_{0.03}O_3$. Furthermore, the emergence of spontaneous electric polarization accompanied by pronounced ME effects has been reported in $Sr_{1-x}Ba_xMnO_3$ [7]. Notably, the magnitude of the observed polarization is comparable to that of the classical ferroelectric $BaTiO_3$ [7]. Additionally, first-principles calculations have predicted a ferroelectric ground state in both the antiferromagnetic 2H phase and the hypothetical ideal cubic perovskite phase of $BaMnO_3$ [8, 9]. These studies suggest that the asymmetric local environment of Mn ions within face-sharing MnO_6 octahedra induces an off-centering displacement of Mn^{4+} ions along the *c*-axis, giving rise to electric polarization—analogous to the mechanisms in conventional multiferroics [7-9]. Moreover, spin–phonon coupling has been shown to play a pivotal role in the ME interactions within these systems [6, 10].

As can be noticed, another intriguing feature of $BaMnO_{3-\delta}$ is its structural instability which can be triggered by numerous factors such as oxygen deficiency, chemical substitution, temperature fluctuations, and applied pressure. Numerous hexagonal and rhombohedral polymorphs, distinguished by varying ratios of corner-sharing and face-sharing octahedra, have been observed [11,12]. As the concentration of oxygen vacancies increases, the proportion of corner-sharing to face-sharing octahedra rises, driving successive structural phase transitions: 2H → 15R → 8H → 9R → 6H → 10H → 4H [11, 12]. Furthermore, a similar trend in polymorphic evolution -15R → 8H → 9R → 10H → 12R - has been reported upon Ti substitution [11]. An increased fraction of corner-sharing octahedra in $BaMnO_3$ has also been observed under compression [13]. At high temperatures, the 2H structure of $BaMnO_3$ undergoes a pressure-induced transformation to the 9R type around 5 GPa, followed by transitions to the 4H and 6H phases at 9 and 20 GPa, respectively [13, 14]. Recent theoretical investigations indicate that the perovskite polymorphs of $BaMnO_3$, consisting exclusively of corner-sharing octahedra, can be stabilized over its rhombohedral and hexagonal counterparts at pressures higher than 20 GPa [15].

Interestingly, strong spin–phonon coupling has also been observed in the 9R phase of the Ti-doped $BaMnO_3$ system ($BaMn_{1-x}Ti_xO_3$) [16, 17], further underscoring the potential of this material for exploring magnetoelectric coupling phenomena. However, the pressure-induced behavior of this phase has not yet been explored. Additionally, structural and electronic phase transitions have been frequently observed in strongly correlated systems such as Mn_3O_4 [18], RMn_2O_5 [19, 20], $Ca_3Co_2O_6$ [21], and etc. On the hand, Kozlenko et al., demonstrated that in $BaMn_{1-x}Ti_xO_3$, the single-phase 9R structure can be stabilized only within a narrow Ti doping range around $x = 0.15$ [11]. Therefore, in this work, we prepared a single-phase 9R $BaMn_{0.85}Ti_{0.15}O_3$ sample and investigated its pressure-dependent behavior using a combination of X-ray diffraction and Raman spectroscopy.

2. Experimental Details

Single-phase polycrystalline $BaMn_{0.85}Ti_{0.15}O_3$ (BMTO) sample was prepared by the conventional solid-state reaction method from mixtures of high-purity precursors $BaCO_3$, Mn_2O_3, and TiO_2 (purchased from Sigma Aldrich, purities ≥ 99.9%). The starting materials were weighed in stoichiometric proportions, thoroughly mixed, and calcined at 1,050 °C for 24 hours. The calcined powders were then pressed into pellets and sintered at 1300 °C for 5 hours in air. The phase composition was analyzed using a Bruker D8 Advance Eco X-ray diffractometer (equipped with a Cu-K_α radiation source: λ_1 = 1.5406 Å, λ_2 = 1.5444 Å, and their intensity ratio I_2/I_1 = 0.48). The sample's morphological properties were examined by scanning electron microscopy (SEM).

High-pressure angle-dispersive synchrotron X-ray diffraction (XRD) measurements were performed up to 20.7 GPa at ambient temperature on Beamline P02.2 at PETRA III, Deutsches Elektronen-Synchrotron DESY (Germany) [22]. The diffraction data were recorded using a flat-panel XRD 1621 detector (PerkinElmer), equipped with a ScI scintillator and an amorphous silicon sensor, positioned 402.33 mm from the sample. Monochromatic X-rays with a wavelength of λ = 0.29118 Å were used for the measurements. The obtained two-dimensional diffraction images were converted into one-dimensional diffraction patterns using the FIT2D software package [23]. Structural analysis of the diffraction data was conducted using the Rietveld refinement method implemented in the FullProf Suite [24]. Raman spectroscopy measurements were conducted at ambient temperature under pressures up to 32.6 GPa, using a LabRam spectrometer equipped with a 632.8 nm He-Ne excitation laser. Both XRD and Raman measurements were performed using a diamond anvil cell, with neon gas used as the pressure-transmitting medium [25]. The ruby fluorescence method was used for pressure determination.

3. Results and Discussion

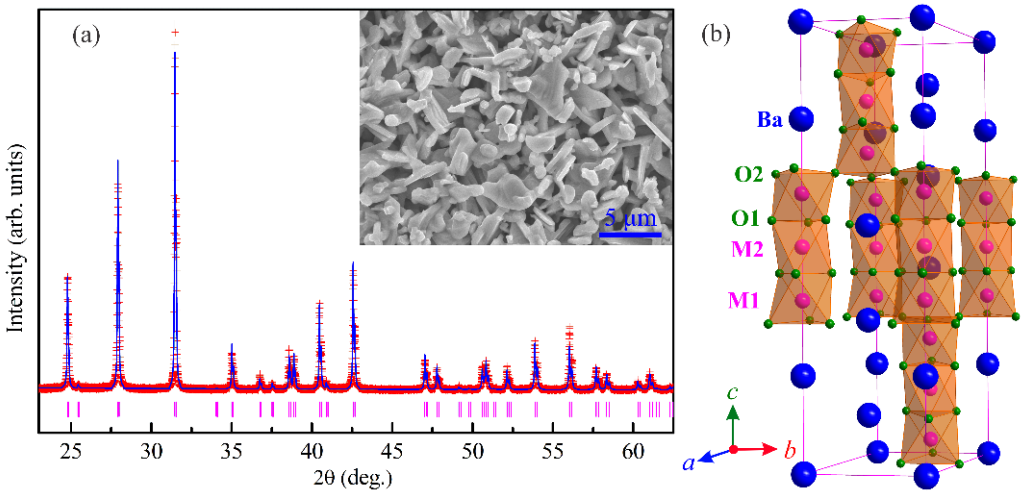

Figure 1. a) XRD pattern of the BMTO sample collected under ambient conditions using a Cu Kα radiation source, along with the corresponding fitting curve. The indices of the most prominent peaks are indicated. Inset: SEM image of the BMTO sample; b) Illustration of the 9R crystal structure.

The phase composition of the prepared sample was examined via the Rietveld refinement of the XRD pattern collected under ambient conditions. As seen in Fig. 1a, the pattern can be fully indexed to a single rhombohedral $R\bar{3}m$ phase with unit-cell parameters a = 9.6784(2) Å and c = 20.9845(9) Å

(hexagonal setting) as shown in Fig. 1b, consistent with values reported in earlier studies [11, 26, 27]. Moreover, the Rietveld refinement employing the structural model previously reported for this 9R phase [11, 26, 27] provided a satisfactory fit to the experimental data, indicating the single-phase nature of the sample.

As revealed by the SEM image, the BMTO sample consists of irregularly shaped particles, of which rod-shaped particles exhibiting sharp edges and corners predominating and randomly oriented (see inset of Fig. 1a). The rods display a broad length distribution ranging from approximately 0.8 μm to 4.5 μm. The particles adhere well to each other, forming large voids within the structure.

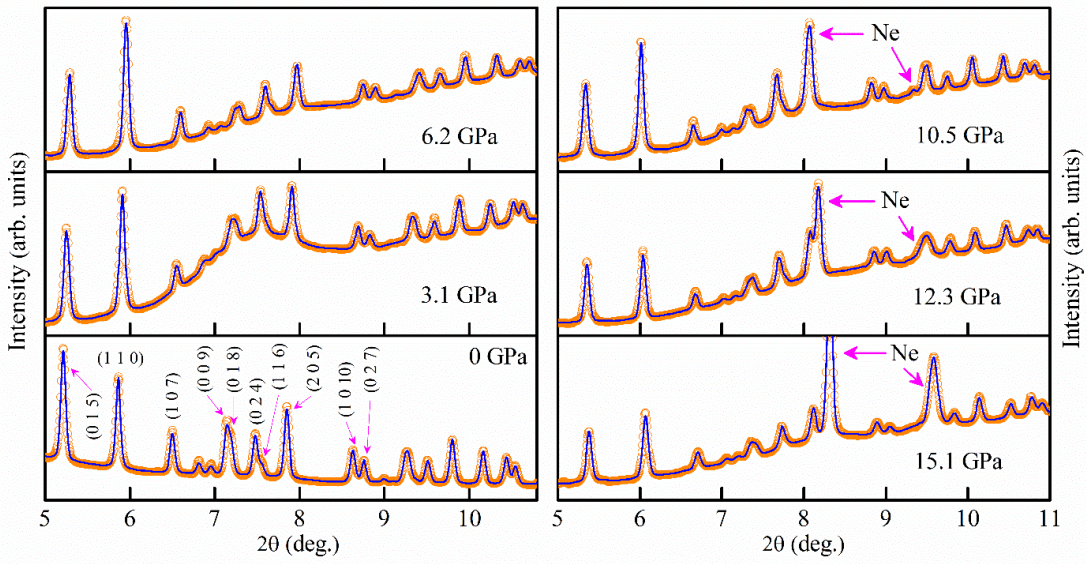

Figure 2. Synchrotron XRD patterns of the BMTO sample (symbols) collected at ambient temperature and selected pressures, along with the corresponding fitting curves. The indices of most prominent peaks are indicated for the pattern collected at 0 GPa. Intense peaks originating from crystalline neon are marked with the symbol "Ne".

Furthermore, the evolution of the 9R phase of BMTO under compression was investigated using synchrotron X-ray diffraction under pressures up to 20.7 GPa, as illustrated in Fig. 2. Data analysis confirmed that the initial 9R phase remained stable across the whole pressure range. At high pressures ($P \geq 10.5$ GPa), along with the characteristic peaks of the 9H phase, additional peaks at 2θ ~8.2° and 9.3° as marked with the symbol "Ne" were observed in the XRD patterns. The data analysis indicates that these peaks correspond to the cubic phase of crystalline neon [28]. The pressure dependence of the lattice parameters and unit-cell volume is presented in Fig. 3. It is important to mention that both lattice parameters display anomalies at around 9 GPa. In particular, the a parameter shows a significant reduction in its average compressibility, defined as $k_a = -(1/a_0)(da/dP)_T$, decreasing from 0.0025 to 0.0017 GPa^{-1} across the critical point. Similarly, k_c decreases from 0.0021 to 0.0014 GPa^{-1}. Additionally, the ratio c/a increases almost linearly and slightly, from 3.765 for 0 GPa to 3.723 for 20.7 GPa, indicating a slight anisotropic lattice compression, with the c-axis being less compressible. This anisotropic compressibility can be attributed to the intrinsic structural anisotropy of the 9R crystal structure, which features face-sharing (Mn/Ti)O_6 octahedra along the c-axis, where strong anisotropic interactions occur (Fig. 1b).

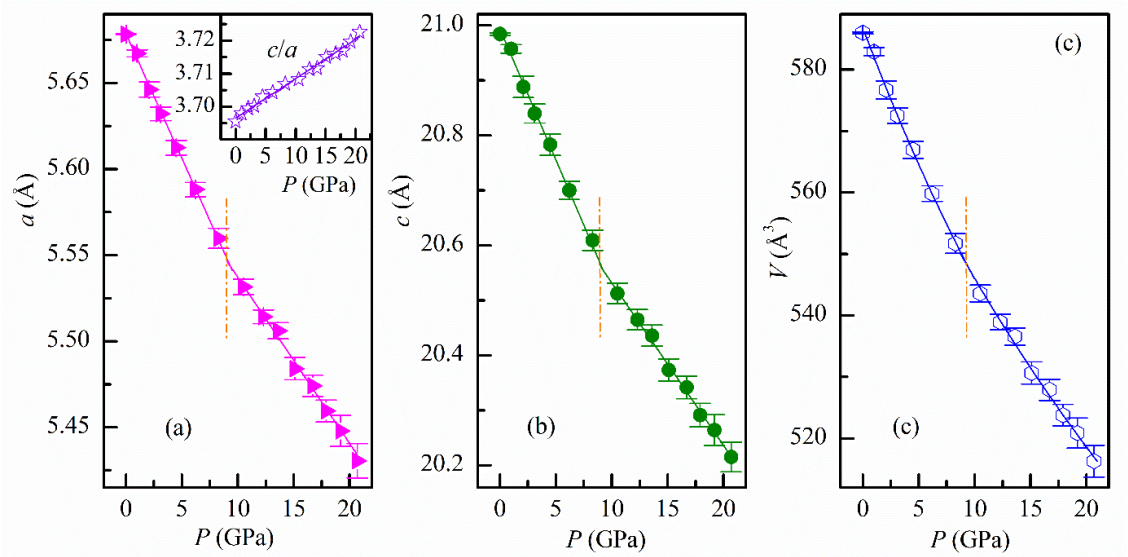

Figure 3. Pressure-dependent evolution of the lattice parameters a (a), c (b), and unit-cell volume V (c) for the BMTO sample, along with their respective fitted curves using the BM equation of state.

Generally, the lattice compressibility data can be fitted by the third-order Birch–Murnaghan (BM) equation of state [29]: $P = \frac{3}{2}B_0(x^{-7/3} - x^{-5/3})[1 + \frac{3}{4}(B' - 4)(x^{-2/3} - 1)]$ (1), where $x = V/V_0$ is the relative volume change, V_0 is the unit cell volume at $P = 0$; B_0 and B' are the bulk modulus, $B_0 = -V(dP/dV)_T$, and its pressure derivative $B' = (dB_0/dP)_T$, respectively. However, since B_0 and B' are often strongly correlated, leading to significant variability in reported values across different measurements for many oxides [21, 30]. Therefore, to ensure more consistent comparison of compressibility data and to facilitate the monitoring of phase transitions, a common approach is to fix $B' = 4$, i.e., applying the second-order Birch-Murnaghan equation of state [19, 21, 30]. Following this approach, for $B' = 4$, the calculated value of B_0 is 120(2) GPa for the pressure range below 9 GPa, increasing to 137(5) GPa above this critical point. Notably, the obtained experimental values B_0 are comparable to those reported for other face-sharing 4H and 6H polymorphs of $SrMnO_3$, which are 115.6(11) GPa and 143.7(17) GPa, respectively [31].

Furthermore, to elucidate the origin of the pressure-induced structural anomalies observed in the BMTO sample, Raman scattering measurements were carried out at room temperature under compression up to 32.6 GPa, as depicted in Fig. 4. At ambient-conditions, nine Raman peaks 258.9, 322.8, 403.0, 423.0, 456.9, 511.2, 528.8, 563.6, and 634.5 cm^{-1} were observed, consistent with previous works [10, 11, 17]. According to group theory, the 9R crystal structure has 9 Raman active modes, $\Gamma = 4A_{1g} + 5E_g$ [11, 32], including A_{1g} and E_g associated with vibrations of Ba, A_{1g} and E_g of Mn/Ti, and $2A_{1g}$ and $3E_g$ of O. It is worth noting that only the O1 and M1 sites contribute to Raman-active phonon modes, while the O2 and M2 sites remain stationary [17, 32, 33]. Additionally, since the vibration modes of Ba ions are expected to occur below 200 cm^{-1} [10, 32], the observation of more Raman modes than theoretically predicted may be attributed to cation disorder. According to Refs. [10, 11, 17, 33], the modes at 258.9 and 322.8 cm^{-1} are primarily associated with vibrations of Mn/Ti ions. The higher-frequency modes are mainly associated with oxygen vibrations: the highest-frequency mode at 634.5 cm^{-1} and the modes in the 511 – 563 cm^{-1} can be assigned to breathing and stretching vibrations of oxygen octahedra, respectively [10, 11, 17, 33]. The remaining modes at 403.0, 423.0, and 456.9 cm^{-1} are attributed to bending vibrations of oxygen octahedra [10, 11, 17, 33].

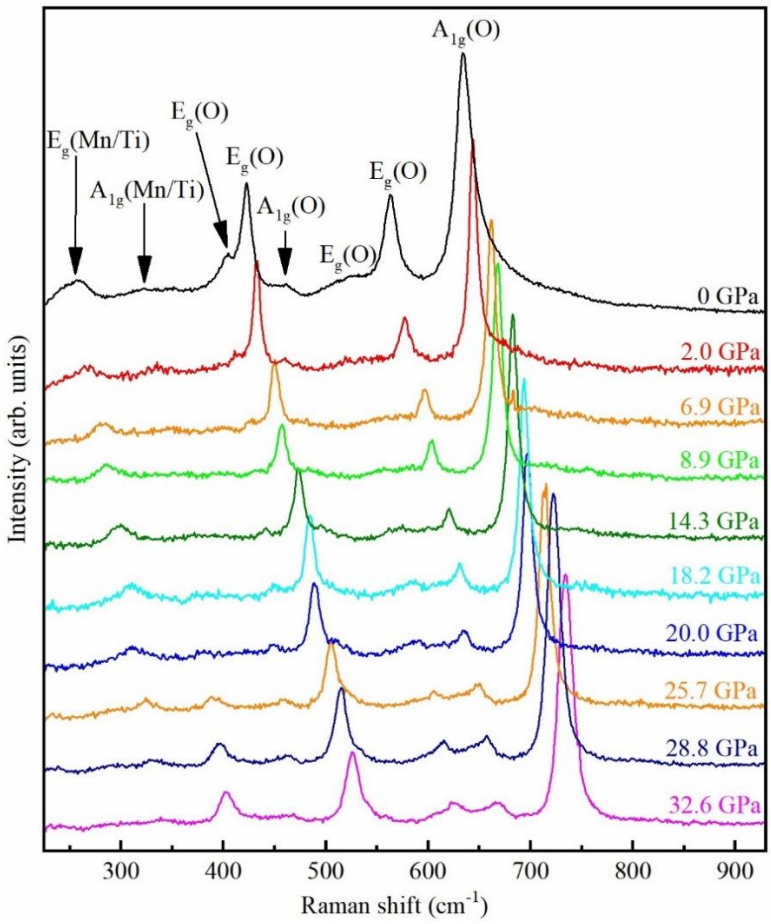

Figure 4. Raman spectra of the BMTO sample measured at room temperature under selected pressures.

As depicted in Fig. 4, all Raman modes persist under compression up to 32.6 GPa, consistent with the stability of the 9R symmetry as reported by the structural investigation presented above. Additionally, above 18.2 GPa, a weak mode with ν = 565.7 cm^{-1} becomes detectable, which may be obscured at lower pressures due to the overlap with other modes. Moreover, the pressure dependence of these Raman modes' frequency is determined and illustrated in Fig. 5. All Raman modes shift towards higher frequencies upon compression. Interestingly, similar to the lattice parameters, all these curves exhibit anomalous behavior around 9 GPa, as evidenced by changes in their slope dv_i/dP and in the mode-Grüneisen parameter $\gamma_i = (B_0/v_i)(dv_i/dP)$, as listed in Table I. Notably, unusual evolutions in the relative intensities of the transition-metal vibration modes are observed (Fig. 4). In particular, the stronger mode at ν = 258.9 cm^{-1} (at 0 GPa) remains almost unchanged up to 18.2 GPa, then gradually weakens under further compression. In contrast, the weaker mode at 322.8 cm^{-1} (at 0 GPa) diminishes and disappears around 8.9 GPa. However, above 18.2 GPa, this mode reappears and strengthens significantly with increasing pressure, eventually becoming more dominant than the lower-frequency mode. These lower- and higher-frequency modes are associated with the vibrations of Mn/Ti ions in the *ab* plane and along the *c* axis, respectively [32]. Therefore, the observations confirm the occurrence the pressure-induced isostructural transformation in BMTO, which is primarily associated with changes in local structural properties related to Mn/Ti vibrations.

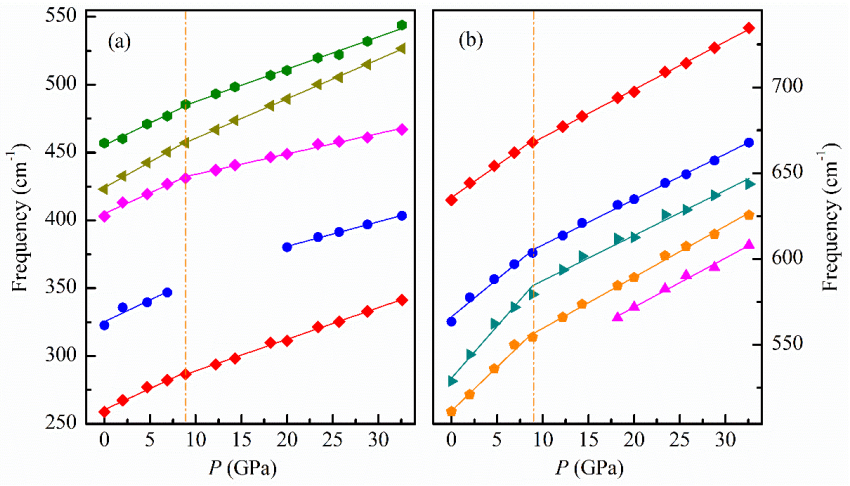

Figure 5. Pressure dependence of vibrational-mode frequencies of the BMTO sample, along with their linear interpolations.

4. Conclusion

In this work, the high-pressure structural and vibrational behavior of BMTO was systematically investigated. High-pressure XRD measurements reveal that the 9R structure remains stable up to 20.7 GPa but undergoes slight anisotropic lattice compression, with the *c*-axis being less compressible due to the intrinsic structural anisotropy. The pressure dependences of all lattice parameters demonstrate anomalies around 9 GPa, indicating a pressure-induced isostructural transformation. This transition is further supported by anomalies in the Raman mode frequencies and by significant changes in the intensity and evolution of Raman-active modes associated with Mn/Ti vibrations (Table 1). These findings suggest pressure-driven rearrangements in the local bonding environment within the Mn/Ti–O octahedral framework, primarily involving Mn/Ti vibrations. To gain deeper insight into the observed phenomena, further theoretical analysis is essential to elucidate their microscopic origin.

Table 1. Pressure coefficients dv_i/dP and mode Grüneisen parameters γ_i of the observed Raman modes in BMTO across different pressure ranges.

v_i (cm^{-1})	dvi/dP (cm^{-1}/GPa)		$\gamma_i = (B_0/v_i)(dv_i/dP)$	
	$P \leq 8.9$ GPa	$P \geq 8.9$ GPa	$P \leq 8.9$ GPa	$P \geq 8.9$ GPa
258.9 (0 GPa)	3.109	2.330	1.367	1.019
322.8 (0 GPa)	3.204	1.815	1.148	0.634
403.0 (0 GPa)	3.058	1.506	0.878	0.459
423.0(0 GPa)	3.785	2.908	1.032	0.811
456.9 (0 GPa)	3.259	2.384	0.832	0.636
565.7 (18.2 GPa)	-	2.859	-	0.669
511.2 (0 GPa)	5.113	2.977	1.151	0.692
528.8 (0 GPa)	5.696	2.635	1.232	0.589
563.6 (0 GPa)	4.379	2.649	0.900	0.571
634.5 (0 GPa)	3.741	2.788	0.689	0.545

Acknowledgments

This work has been funded by Vietnam National Foundation for Science and Technology Development (NAFOSTED) under grant number 103.02-2021.70. We acknowledge the Deutsches Elektronen-Synchrotron (DESY) for the provision of experimental facilities.

References

[1] J. V. D. Brink, D. I. Khomskii, Multiferroicity Due to Charge Ordering, Journal of Physics: Condensed Matter, Vol. 20, No. 43, 2008, pp. 434217, https://doi.org/10.1088/0953-8984/20/43/434217.

[2] S. W. W. Cheong, M. Mostovoy, Multiferroics: A Magnetic Twist for Ferroelectricity, Nature Materials, Vol. 6, 2007, pp. 13-20, https://doi.org/10.1038/nmat1804.

[3] T. Kimura, T. Goto, H. Shintani, K. Ishizaka, T. Arima, Y. Tokura, Magnetic Control of Ferroelectric Polarization, Nature, Vol. 426, 2003, pp. 55-58, https://doi.org/10.1038/nature02018.

[4] M. Fiebig, T. Lottermoser, D. Meier, M. Trassin, The Evolution of Multiferroics, Nature Reviews Materials, Vol. 1, 2016, pp. 16046, https://doi.org/10.1038/natrevmats.2016.46.

[5] G. Lawes, A. B. Harris, T. Kimura, N. Rogado, R. J. Cava, A. Aharony, O. E. Wohlman, T. Yildirim, M. Kenzelmann, C. Broholm, A. P. Ramirez, Magnetically Driven Ferroelectric Order in $Ni_3V_2O_8$, Physical Review Letters, Vol. 95, No. 8, 2005, pp. 087205, https://doi.org/10.1103/PhysRevLett.95.087205.

[6] O. B. Korneta, T. F. Qi, M. Ge, S. Parkin, L. E. De Long, P. Schlottmann, G. Cao, Correlated Giant Dielectric Peaks and Antiferromagnetic Transitions Near Room Temperature in Pure and Alkali-doped $BaMnO_{3-\delta}$, Journal of Physics: Condensed Matter, Vol. 23, No. 43, 2011, pp. 435901, https://doi.org/10.1088/0953-8984/23/43/435901.

[7] H. Sakai, J. Fujioka, T. Fukuda, D. Okuyama, D. Hashizume, F. Kagawa, H. Nakao, Y. Murakami, T. Arima, A. Q. R. Baron, Y. Taguchi, Y. Tokura, Displacement-Type Ferroelectricity with Off-center Magnetic Ions in Perovskite $Sr_{1-x}Ba_xMnO_3$, Physical Review Letters, Vol. 107, No. 13, 2011, pp. 137601, https://doi.org/10.1103/PhysRevLett.107.137601.

[8] J. Varignon, P. Ghosez, Improper Ferroelectricity and Multiferroism in 2H-$BaMnO_3$, Physical Review B, Vol. 87, No. 14, 2013, pp. 140403, https://doi.org/10.1103/PhysRevB.87.140403.

[9] J. M. Rondinelli, A. S. Eidelson, N. A. Spaldin, Non-d^0 Mn-driven Ferroelectricity in Antiferromagnetic $BaMnO_3$, Physical Review B, Vol. 79, No. 20, 2009, pp. 205119, https://doi.org/10.1103/PhysRevB.79.205119.

[10] B. Poojitha, A. Rathore, A. Kumar, S. Saha, Signatures of Magnetostriction and Spin-phonon Coupling in Magnetoelectric Hexagonal 15R-$BaMnO_3$, Physical Review B, Vol. 102, No. 13, 2020, pp. 134436, https://doi.org/10.1103/PhysRevB.102.134436.

[11] D. P. Kozlenko, N. T. Dang, T. L. Phan, S. E. Kichanov, L. H. Khiem, S. G. Jabarov, T. A. Tran, T. V. Manh, A. T. Le, T. K. Nguyen, B. N. Savenko, The Structural, Magnetic and Vibrational Properties of Ti-doped $BaMnO_3$, Journal of Alloys and Compounds, Vol. 695, 2017, pp. 2539-2548, https://doi.org/10.1016/j.jallcom.2016.11.159.

[12] N. V. Tarakina, A. P. Tyutyunnik, G. V. Bazuev, A. D. Vasilev, C. Gould, I. V. Nikolaenko, I. F. Berger, Synthesis and Crystal Structure of a New Hexagonal Perovskite 7H-$Ba_7Li_{1.75}Mn_{3.5}O_{15.75}$ with Mn^{4+}/Mn^{5+} Charge Distribution, Dalton Transactions, Vol. 44, No. 42, 2015, pp. 18527-18535, https://doi.org/10.1039/C5DT01528F.

[13] Y. Syono, S. I. Akimoto, K. Kohn, Structure Relations of Hexagonal Perovskite-Like Compounds ABX_3 at High Pressure, Journal of the Physical Society of Japan, Vol. 26, No. 4, 1969, PP. 993-999, https://doi.org/10.1143/JPSJ.26.993.

[14] S. Qin, Y. Y. Chin, B. Zhou, Z. Liu, X. Ye, J. Guo, G. Liu, C. T. Chen, Z. Hu, Y. Long, High-Pressure Synthesis and Magnetism of the 4H-$BaMnO_3$ Single Crystal and Its 6H-Type Polymorph, Inorganic Chemistry, Vol. 60, No. 21, 2021, pp. 16308-16315, https://doi.org/10.1021/acs.inorgchem.1c02155.

[15] H. Chen, A. J. Millis, Phase Diagram of $Sr_{1-x}Ba_xMnO_3$ as a Function of Chemical Doping, Epitaxial Strain, and External Pressure, Physical Review B, Vol. 94, No. 16, 2016, pp. 165106, https://doi.org/10.1103/PhysRevB.94.165106.

[16] P. Thakur, S. Kumari, S. Chaudhary, N. Sharma, M. Lal, Multifunctional Tuning of Structural, Dielectric, and Magnetic Properties of Ti-doped $BaMnO_3$ Ceramics, Emergent Materials, Vol. 7, 2024, pp. 1733-1752, https://doi.org/10.1007/s42247-024-00689-y.

[17] B. Poojitha, A. Rathore, S. Saha, Spin-Phonon Coupling in Sr and Ti Incorporated 9R-$BaMnO_3$, Journal of Magnetism and Magnetic Materials, Vol. 483, 2019, pp. 212–218, https://doi.org/10.1016/j.jmmm.2019.03.114.
[18] D. P. Kozlenko, N. T. Dang, S. E. Kichanov, L. T. P. Thao, A. V. Rutkaukas, E. V. Lukin, B. N. Savenko, N. Tran, D. T. Khan, L. V. T. Son, L. H. Khiem, B. W. Lee, T. L. Phan, N. L. Phan, N. T. Tho, N. N. Hieu, T. A. Tran, M. H. Phan, High Pressure Enhanced Magnetic Ordering and Magnetostructural Coupling in the Geometrically Frustrated Spinel Mn_3O_4, Physical Review B, Vol. 105, No. 9, 2022, pp. 094430, https://doi.org/10.1103/PhysRevB.105.094430.
[19] K. K. Pandey, H. K. Poswal, R. Kumar, S. M. Sharma, High Pressure Iso-structural Phase Transition in $BiMn_2O_5$, Journal of Physics: Condensed Matter, Vol. 25, No. 32, 2013, pp. 325401, https://doi.org/10.1088/0953-8984/25/32/325401.
[20] D. P. Kozlenko, N. T. Dang, S. E. Kichanov, E. V. Lukin, A. M. Pashayev, A. I. Mammadov, S. H. Jabarov, L. S. Dubrovinsky, H. P. Liermann, W. Morgenroth, R. Z. Mehdiyeva, V. G. Smotrakov, B. N. Savenko, Competing Magnetic and Structural States in Multiferroic YMn_2O_5 at High Pressure, Physical Review B, Vol. 92, No. 13, 2015, pp. 134409, https://doi.org/10.1103/PhysRevB.92.134409.
[21] D. T. Khan, D. P. Kozlenko, S. E. Kichanov, E. V. Lukin, T. N. Nguyen, N. T. Tho, V. T. Nguyen, T. A. Tran, N. L. Phan, T. P. Hoang, S. H. Jabarov, A. V. Rutkauskas, N. T. Dang, Revealing the Electronic Origin of Pressure-Induced Isostructural Transformations in $Ca_3Co_2O_6$, Journal of Electronic Materials, Vol. 54, 2025, pp. 3651-3662, https://doi.org/10.1007/s11664-025-11742-9.
[22] H. P. Liermann, W. Morgenroth, A. Ehnes, A. Berghäuser, B. Winkler, H. Franz, E. Weckert, The Extreme Conditions Beamline at PETRA III, DESY: Possibilities to Conduct Time Resolved Monochromatic Diffraction Experiments in Dynamic and Laser Heated DAC, Journal of Physics: Conference Series, Vol. 215, 2010, pp. 012029, https://doi.org/10.1088/1742-6596/215/1/012029.
[23] A. P. Hammersley, S. O. Svensson, M. Hanfland, A. N. Fitch, D. Häusermann, Two-dimensional Detector Software: From Real Detector to Idealised Image or Two-Theta Scan, High Pressure Research, Vol. 14, No. 4-6, 1996, pp. 235-248, https://doi.org/10.1080/08957959608201408.
[24] J. R. Carvajal, Recent Advances in Magnetic Structure Determination by Neutron Powder Diffraction, P Physica B: Condensed Matter, Vol. 192, No. 1-2, 1993, pp. 55-69, https://doi.org/10.1016/0921-4526(93)90108-I.
[25] N. Dubrovinskaia, L. Dubrovinsky, Whole-cell Heater for The Diamond Anvil Cell, Review of Scientific Instruments, Vol. 74, No. 7, 2003, pp. 3433-3437, https://doi.org/10.1063/1.1578151.
[26] J. J. Adkin, M. A. Hayward, $BaMnO_{3-x}$ Revisited: A Structural and Magnetic Study, Chemistry of Materials, Vol. 19, No. 4, 2007, pp. 755-762, https://doi.org/10.1021/cm062055r.
[27] L. Miranda, D.C. Sinclair, M. Hernando, A. Varela, J. Ramírez-Castellanos, K. Boulahya, J.M. González-Calbet, M. Parras, Polytypism in The $BaMn_{0.85}Ti_{0.15}O_{3-\delta}$ System ($0.07 \leq \delta \leq 0.34$). Structural, Magnetic, and Electrical Characterization of The 9R-polymorph, Chemistry of Materials, Vol. 22, No. 14, 2010, pp. 4320-4327, https://doi.org/10.1021/cm1012735.
[28] L.W. Finger, R. M. Hazen, G. Zou, H. K. Mao, P. M. Bell, Structure and Compression of Crystalline Argon and Neon at High Pressure and Room Temperature, Applied Physics Lettes, Vol. 39, No. 11, 1981, pp. 892-894, https://doi.org/10.1063/1.92597.
[29] M. Frogley, J. Sly, D. Dunstan, Pressure Dependence of the Direct Band Gap in Tetrahedral Semiconductors, Physical Review B, Vol. 58, No. 19, 1998, pp. 12579-12582, https://doi.org/10.1103/PhysRevB.58.12579.
[30] D. Errandonea, R. S. Kumar, F.J. Manjón, V. V. Ursaki, E. V. Rusu, Post-spinel Transformations and Equation of State in $ZnGa_2O_4$: Determination at High Pressure by *In Situ* X-ray Diffraction, Physical Review B, Vol. 79, No. 2, 2009, pp. 024103, https://doi.org/10.1103/PhysRevB.79.024103.
[31] M. B. Nielsen, D. Ceresoli, P. Parisiades, V. B. Prakapenka, T. Yu, Y. Wang, M. Bremholm, Phase Stability of The $SrMnO_3$ Hexagonal Perovskite System at High Pressure and Temperature, Physical Review B, Vol. 90, No. 21, 2014, pp. 214101, https://doi.org/10.1103/PhysRevB.90.214101.
[32] Y. S. Lee, T. W. Noh, J. H. Park, K. B. Lee, G. Cao, J. E. Crow, M. K. Lee, C. B. Eom, E. J. Oh, I. S. Yang, Temperature-Dependent Raman Spectroscopy in $BaRuO_3$ Systems, Physical Review. B, Vol. 65, No. 23, 2002, pp. 235113, https://doi.org/10.1103/PhysRevB.65.235113.
[33] P. Bommareddy, A. Kumar, A. Rathore, D. Negi, S. Saha, Engineering Crystal Structure and Spin-phonon Coupling in $Ba_{1-x}Sr_xMnO_3$, Journal of Magnetism and Magnetic Materials, Vol. 541, 2022, pp. 168539, https://doi.org/10.1016/j.jmmm.2021.168539.